ADVANCED MATERIALS
www.advmat.de

Microfluidic Oxidation of Graphite in Two Minutes with Capability of Real-Time Monitoring

*Chuanren Ye, Gang Wang, Hong Yuan, Jieyun Li, Kun Ni, Fei Pan, Minghao Guo, Yanhong Wu, Hengxing Ji, Fan Zhang, Bill Qu, Zhiyong Tang, and Yanwu Zhu**

Graphite oxide and its exfoliated counterpart, graphene oxide, are important precursors for the large-scale production of graphene-based materials and many relevant applications. The current batch-style preparation of graphite oxide suffers from safety concern, long reaction time, and nonuniform product quality, due to the large volume of reactors and slow energy exchange. Reaction in microchannels can largely enhance the oxidization efficiency of graphite due to the enhanced mass transfer and extremely quick energy exchange, by which the controllable oxidization of graphite is achieved in ≈2 min. Comprehensive characterizations show that the graphene oxide obtained through the microfluidic strategy has features like those prepared in laboratory beakers and industrial reactors, yet with the higher oxidization degree and more epoxy groups. More importantly, the microfluidic preparation allows for on-line monitoring of the oxidization by Raman spectroscopy, ready for the dynamical control of reaction condition and product quality. The capability of continuous preparation is also demonstrated by showing the assembly of fibers and reduction of graphene oxide in microfluidic channels, and the applicability of graphene oxide prepared from the microfluidic strategy for thermally and electrically conductive films.

1. Introduction

Graphene oxide (GO) can be considered as graphene skeleton decorated with abundant oxygen-containing functional groups, among which typical ones such as epoxy and hydroxyl are covalently bonded to the basal plane and carboxyl to the edges. The hydrophilic functional groups ensure the favorable dispersion of GO in a variety of polar solvents and thus an excellent solution-based processing capability,[1] which benefits further the assembly of GO into multiple macroscopic structures such as aerogels,[2] films/papers,[3] and fibers.[2,4] Bridging the interesting properties of intrinsic graphene and practically useful products, GO and GO-derived materials have been actively investigated for applications such as energy storage,[5,6] water treatment,[7] optoelectronics,[8] polymer composites,[9] and biomedicine.[10] Above all, GO can be readily prepared from graphite oxide, and reduced via several methods to partially recover the conjugation.[11]

Since the pioneering work done by Brodie in 1859[12] and Staudenmaier in 1898,[13] the oxidation of graphite has been explored with various chemical or electrochemical methods, among which the Hummers' method first reported in 1958,[14] has become a primary approach to fabricate GO both in fundamental research and industrial production.[15] Nowadays, the traditional Hummers' method has been modified to minimize the generation of toxic gases, e.g., NO_2 and N_2O_4, and to promote the sluggish oxidant interlayer diffusion kinetics as well. $NaNO_3$ has been excluded or replaced by H_3PO_4 to alleviate the safety issue.[16] However, the active oxidant Mn_2O_7, generated by dissolving $KMnO_4$ in concentrated H_2SO_4, is potentially explosive for temperatures exceeding 55 °C,[17] leading to a huge safety concern in industrial production, especially in large volume reactors.[18] On the other hand, the diffusion-controlled oxidization of graphite,[19] typically takes several or tens of hours to obtain a high-yield preparation of GO in beakers.[20] Although the reaction can be speeded up by using strong oxidants like K_2FeO_4, the typical reaction still needs 1 h and the larger amount of oxidant.[21] Electrochemical oxidation could accelerate the diffusion and thus the oxidization by applying a voltage on the pre-intercalated graphite,[22,23] but the bulk

C. Ye, H. Yuan, J. Li, K. Ni, F. Pan, M. Guo, H. Ji, Z. Tang, Y. Zhu
School of Chemistry and Materials Science
University of Science and Technology of China
Hefei 230026, China
E-mail: zhuyanwu@ustc.edu.cn
G. Wang, Z. Tang
CAS Key Laboratory of Low-Carbon Conversion Science and Engineering
Shanghai Advanced Research Institute
Chinese Academy of Sciences
Shanghai 201210, China
G. Wang, Z. Tang
University of the Chinese Academy of Sciences
Beijing 100049, China
Y. Wu, B. Qu
The Sixth Element (Changzhou) Materials Technology Co., Ltd.
Changzhou 213000, China
F. Zhang
School of Chemistry and Chemical Engineering
Shanghai Jiao Tong University
Shanghai 200240, China
The ORCID identification number(s) for the author(s) of this article can be found under https://doi.org/10.1002/adma.202107083.

DOI: 10.1002/adma.202107083

graphite electrode might deteriorate the diffusion in the industrial production along with the oxidization.

The aforementioned challenges are closely associated to the diffusion efficiency of reactants and energy exchange in the benchtop beakers or ton-scale industrial reactors, which also bring problems related to the uniformity and stability of graphite oxide produced.[24] Since the mixing and mass transfer of reactants can be seriously affected by hydrodynamic flow regime,[25] a subtle control of the flow shall help to make the product quality more stable and uniform. In the past two decades, the continuous flow reaction in microchannels has been proved valid in a wide range of fields especially for pharmaceuticals and fine chemistry.[26–28] The small reactor volume and exceedingly fast heat transfer of microreactors minimize the risk involving hazardous reagents.[29] The rapid species transport in the microchannels enables the easier control over the reaction kinetics and provide an opportunity for real-time monitoring, both of which are very challenging in batch-style reactions.[30,31] Taking advantage of high gradient fluid feature in microchannels, Ferrari and co-workers reported the exfoliation of graphite under the high shear rate ($\approx 10^8$ s^{-1}) turbulent flow (in a microchannel with a diameter ≈87 µm),[32] from which few layer graphene platelets with a lateral size of ≈1 µm and a mean thickness of ≈10 nm were obtained in sodium deoxycholate aqueous solution after 70 cycles of processing. By introducing H_3PO_4 microdroplets in a continuous graphite/H_2SO_4 flow, Chen and co-workers reported the partial oxidation of graphite in a T-shaped microchip, and the resulting solution was subsequently conveyed into $KMnO_4$ to complete the oxidation within 2 h.[33] Graphene fibers have been prepared through a microfluid-directed strategy, in which GO was amino-functionalized and assembled into 3D network in a hydrothermal microreactor; the resulting N-doped graphene fibers presented a capacitance of 1132 mF cm^{-2} as micro-supercapacitors.[34] Although the proceedings above, the microfluidic synthesis of graphite oxide towards mass production remains to be investigated towards the higher efficiency and tailorable chemical features.

Herein, we report a scalable, fast, yet intrinsically safe continuous flow synthesis of graphite oxide in microreactors. The enhanced mass transfer and energy exchange accelerate the oxidation to ≈2 mins in the microchannels, several tens of times faster than the traditional Hummers' method in batch-style reactors, due to the synergistic effect of enhanced local shear and the rotational motion of graphite flakes in microchannels. The chemical structure of GO can be efficiently tailored by changing fluidic parameters such as flow velocity, resident time, and reactor configuration. Through Raman spectroscopy, the oxidation reaction in microchannels is monitored in real time. The capability for the continuous integration of graphite oxide production and post processing all the way in microchannels is demonstrated. GO obtained by microfluidic oxidation is used to prepare electrically and thermally conductive films, further showing the promising applicability of the current strategy.

2. Results and Discussion

We start with the optimization of microchannels to verify the effect of fluidic features. As an accessible and commonly used microchannel, a transparent polyfluoroalkoxy (PFA) capillary with an inner diameter of 1 mm (Figure S1a, Supporting Information) was firstly tried for the continues flow oxidation of graphite. Although the miniaturized dimension can significantly speed up the energy transfer, the laminar flow causes inefficient mixing between graphite and oxidants.[35] Thus, a chip microreactor has been designed, as shown in **Figure 1**a, consisting of heart-shape microreactors connected by diameter-changing channels (geometric details in Figure 1b) sandwiched by two holey plates for temperature control in water (photo in Figure S1b in the Supporting Information). The split-and-recombine structure in the chip would repeatedly stretch and transversely shear the fluids, benefiting the effective mixing in the high-viscosity sulfuric acid.[36] The heart-shape configuration shall promote the generation of secondary flow and avoid the local sedimentary or even blockage due to the presence of graphite particles.[37] The recombine section brings the lower pressure drop in the device and the larger residence volume in the limited space. The trapezoidal structure of the bifurcation area with changing diameter would compress fluids, to enhance the shearing effect and the local pressure gradient. We shall note that, similar designs that introduce obstacles or modified channel geometry like split-recombine structure, grooves and specially designed turns may also promote the diffusion due to the enhanced convection within the microreactor.

Numerical simulations in the concentrated H_2SO_4 flow (velocity: 0.017 m s^{-1}) while without graphite flakes have been carried out to reveal the discrepant fluidic feature. As shown in Figure 1c, a dramatical velocity difference is observed along the flow direction in the chip microchannel, from which the maximum velocity is ≈0.078 m s^{-1} in the convergence unit, much higher than that in the bifurcation unit (≈0.028 m s^{-1}). Correspondingly, the velocity gradient brings about a mean shear rate up to 101.4 s^{-1}, with a maximum value of 429.4 s^{-1} at the narrow segment of the trapezoidal channel in the convergence unit as viewed in Figure 1d. When the velocity is elevated up to a high value, e.g., 0.25 m s^{-1}, the local turbulence starts to appear in the chip microreactor (Figure S2, Supporting Information) but the streamline in the PFA capillary remains parallel to the channel direction even for 1.667 m s^{-1}, as shown in Figure S3 in the Supporting Information. Due to the high shear rate created by the chip microreactor, graphite flakes in H_2SO_4 are rotated in the channels, as recorded and shown in Figure 1e. From the clips we can see that the graphite flake of interest starts to be parallel to the plane of view, then gradually tunes to be perpendicular, eventually back to the plane after 15 s. The trajectory of graphite flakes appears to be along the streamlines while without obvious displacement in the plane perpendicular to the flow direction,[38] as can be seen more clearly in Supporting Movies S1 and S2. Figure 1f schematically shows the parabolic-like velocity profile and the shear rate destitution in the microchannel, which explains the velocity difference at the different streamlines as observed Figure S4 in the Supporting Information. In contrast, the maximum velocity and shear rate in the PFA microchannel are 0.033 m s^{-1} (Figure 1g) and 192.0 s^{-1} (Figure 1h), far lower than those in the chip microchannel.

Based on the analyses above, the chip microreactor has been mainly used for the oxidization of graphite and the PFA capillary (inner diameter: 1 mm, length: 0.5–3 m) was used for

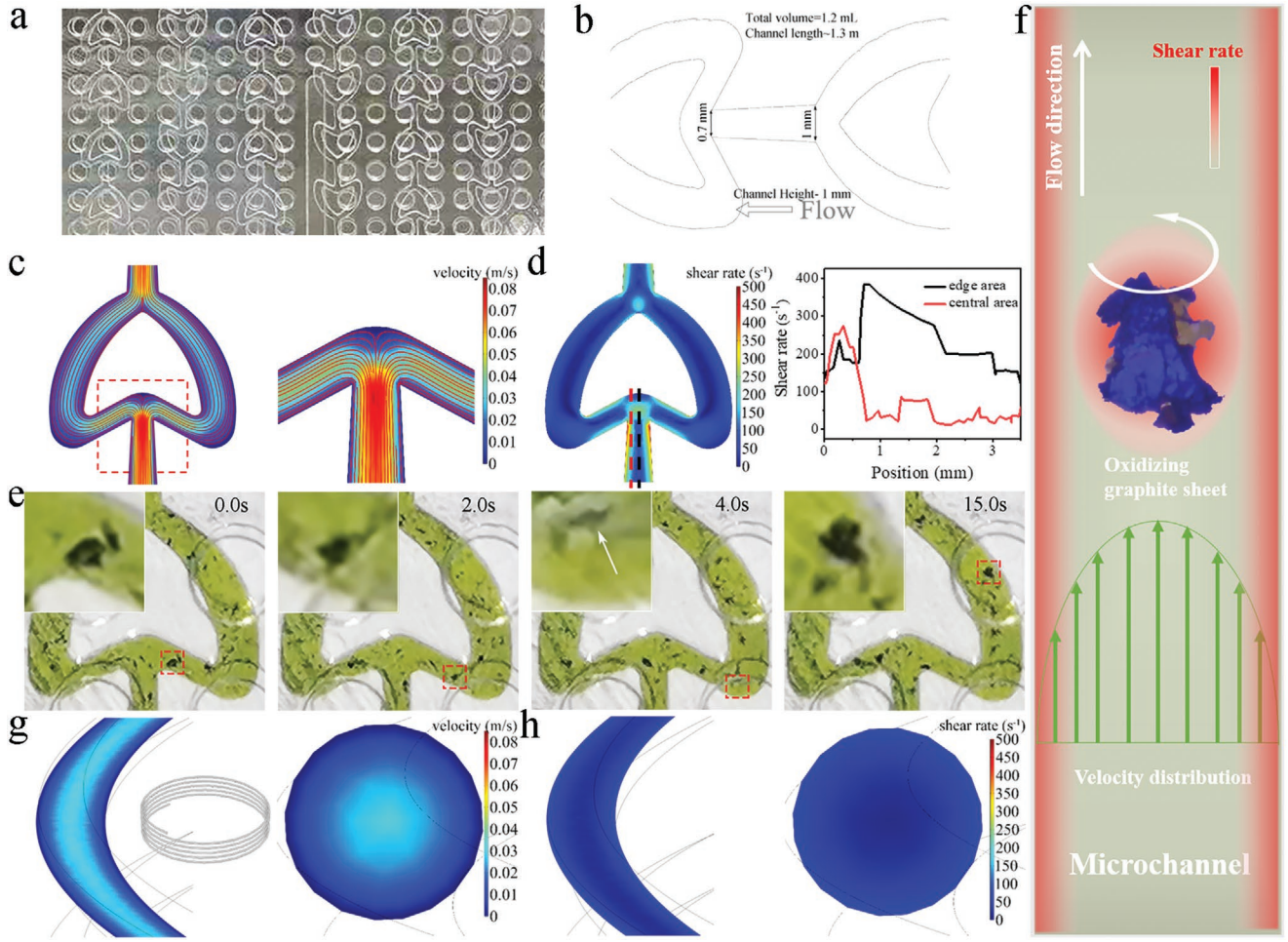

Figure 1. a) Photograph of custom-designed chip microchannels. b) Enlarged channel with size labeled. c,d) Numerical simulations of velocity distribution (enlarged view in the inset) (c) and shear rate distribution (rate values along the dashed line in the central and nearby the edge, respectively, in the inset curves) (d) for bare H_2SO_4 (temperature: 30 °C, flow rate: 0.017 m s^{-1}) in a structural unit of the chip microchannels. e) Rotational motion of graphite flakes recorded in the chip microreactor. f) Schematic indicating the spatial movement of a graphite flake and the distribution of shear rate in the microchannel. g,h) Numerical simulations of velocity distribution (cross section view in the inset) (g) and shear rate distribution (cross section view in the inset) (h) for bare H_2SO_4 in a structural unit of the PFA microchannel.

parameter search in control experiments. In the preparation, expandable graphite (EG), which was obtained by weak oxidization of natural graphite,[39] was used as the main raw material and the characterizations of EG are included in Figure S5 in the Supporting Information. For the preparation of graphite oxide, $KMnO_4$ and EG powders were added to concentrated H_2SO_4 (98 wt%), followed by vigorous mixing for 1 h in an ice-bath to obtain stage-1 graphite intercalation compound (GIC). As the formation of deep blue graphite sulfate only takes several minutes,[19] this process was carried out in a beaker to avoid a vague oxidation control in microchannels in the current research. Then the GIC was pumped into the chip microreactor for oxidization, as shown in **Figure 2**a. The suspensions of graphite oxide were finally obtained, as shown in Figure 2b.

Typically, the residence time of GIC in the chip microreactor was set to 1.2 min corresponding to a flow rate of 1 mL min^{-1}, while the reaction temperature was maintained at 35 °C by immersing the reactor in a water bath. After termination of oxidation and separation of graphite oxide by centrifugation, HCl solution washing was carried out twice by centrifugation, followed by washing with deionized water at 11 000 rpm till the supernatant reached the neutral pH, and a mild ultrasonic exfoliation for 5 min (more details in Experimental Section). The obtained graphite oxide through microfluidic strategy (abbreviated as MfGO) shows a homogeneous dispersion in water without visible precipitates; the diluted suspension owns a clear colloidal feature under laser irradiation (Figure 2c). The exfoliation degree has been evaluated by calculating the mass ratio of GO freeze-dried from the centrifugation supernatant to the total mass; the value of ≈67% (3000 rpm, corresponding to an acceleration of 1006*g*) is comparable with that obtained from the improved Hummers' method such as in Refs. [39,40] In such microchannels, graphite oxide can be continuously produced with a production rate of ≈1.3 g h^{-1} (≈11 kg per year for a 1.2 mL microreactor), more efficient than the case in lab beakers where it usually takes nearly a day to prepare grams of graphite oxide.[16] As estimated, to achieve a production ability of 60 tons per year, the total flow volume in the

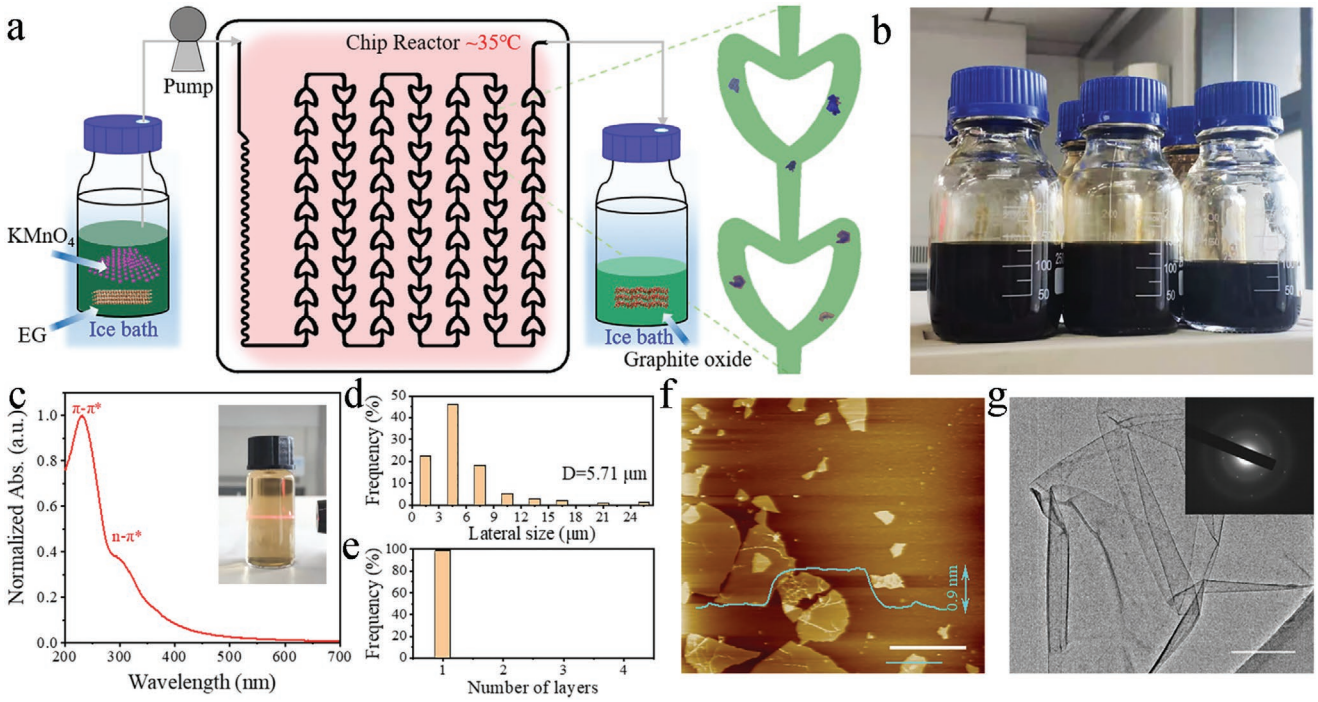

Figure 2. a) Schematics of the experiment setup employed in the microfluidic synthesis of graphite oxide and the enlarged microchannel. b) Optical photo of MfGO aqueous suspensions (2–5 mg mL^{-1}) prepared. c) UV–vis absorption spectrum and optical photo (0.2 mg mL^{-1}, inset) of MfGO suspension. d) Lateral size distribution and e) layer number distribution of MfGO platelets. f) Typical AFM image and height profile of MfGO. g) Typical TEM image of MfGO platelets and SAED pattern (inset). Scale bars: f) 5 μm, g) 0.5 μm.

microreactors is only ≈6.54 L, significantly smaller than the typical reactors required in the traditional production. Moreover, the microfluidic oxidization of graphite can be cooperated with existing technology such continuous mixture of graphite and concentrated H_2SO_4, quick purification by directly separating graphite oxide slurry[39] and other exfoliation methods assisted by industrial equipment, to further improve oxidation efficiency (Table S1, Supporting Information). The improved safety and potential parallel production would further highlight the advantages of the microfluidic strategy.

For comparison, GO was also prepared by the modified Hummers' method in beakers with the same EG as raw material (resulting in samples called HGO). Following the previous report,[41] after $KMnO_4$ was introduced, the mixture was maintained at 35 °C for 2 hours, then water was subsequently added at the elevated temperature of 95 °C for 15 min to prepare HGO. The UV–vis spectroscopy (Figure 2c; Figure S6a, Supporting Information) of the suspensions shows that MfGO owns absorption peaks of π-π^* transition (≈234 nm) and n-π^* transition (≈303 nm) like HGO. The average lateral size of 296 MfGO platelets is ≈5.7 μm based on the scanning electron microscopy (SEM) measurement (Figure 2d; Figure S7a, Supporting Information), much smaller than those of the raw EG (≈119 μm, Figure S5a, Supporting Information) and HGO (≈40 μm, Figure S6b,c, Supporting Information). The atomic force microscopy (AFM) image in Figure 2f shows that MfGO platelets have a thickness of ≈0.9 nm, corresponding to a single layer graphene with oxygen-containing functional groups. Extensive AFM observations of 291 MfGO platelets reveal that the fraction of monolayers is ≈99% (Figure 2e). The straight wrinkles in the transmission electron microscopy (TEM) image (Figure 2g) indicate the crystalline feature of MfGO, confirmed by the selected-area electron diffraction (SAED) pattern in the inset of Figure 2g.

Two samples made through microfluidic synthesis have been analyzed, for which the resident time was set as 1.2 min (flow rate: 1 mL min^{-1}) or 4 min (flow rate: 300 μL min^{-1}), leading to samples named as MfGO-1.2 or MfGO-4.0, respectively. From X-ray photoelectron spectroscopy (XPS) results (**Figure 3**a), we can see that the C/O atomic ratio of MfGO-1.2 is much lower than the typical value for HGO,[22,23] though from the same EG. Four deconvolution peaks in XPS C1s spectra correspond to C=C (≈284.8 eV), C—O (≈286.8 eV), C=O (≈288.1 eV), and O—C=O (≈289.0 eV). The prominent peak of C—O bond in MfGO-1.2 indicates the higher amount of epoxy and hydroxyl groups compared with HGO, in which the C=O peak is relatively stronger (details in Table S2 in the Supporting Information). Longer resident time in microchannels has resulted in even lower C/O atomic ratio, as indicated by the result from MfGO-4.0. The X-ray diffraction (XRD) patterns (Figure 3b) show that the diffraction peak position at 2θ = 10.3° for MfGO-1.2 and MfGO-4.0, corresponding to an interlayer spacing of ≈8.6 Å, slightly larger than that of HGO (7.8 Å). Raman spectra in Figure 3c show that MfGOs and HGO have prominent D (1351cm^{-1}) and G (1593cm^{-1}) peaks,[42] while they all exhibit similar shapes and I_D/I_G values close to 0.90. ^{13}C nuclear magnetic resonance spectrometry (NMR) and Fourier transformed infrared (FTIR) spectrometry were performed to further identify the variety of functional groups. As can be seen from Figure 3d, three main peaks from NMR, namely at 131, 69, and

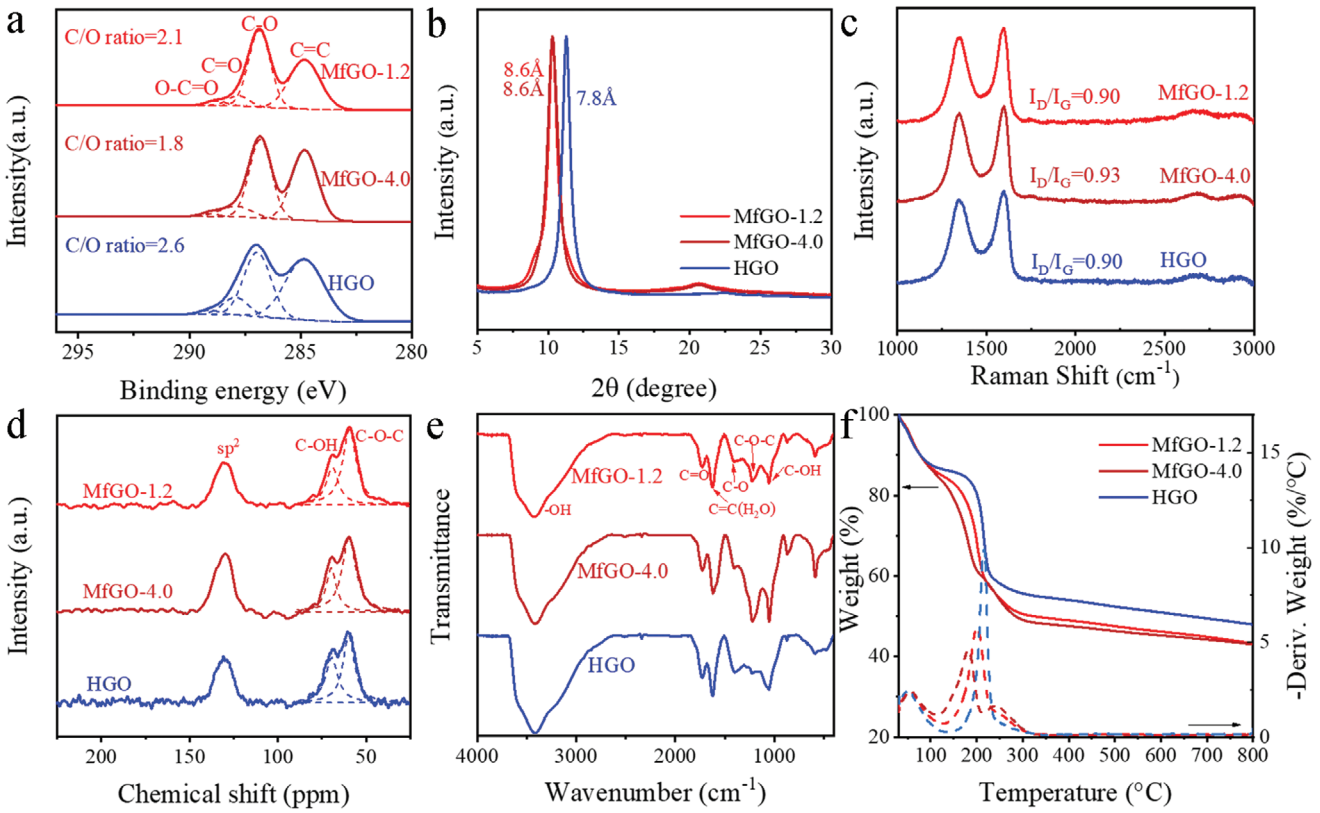

Figure 3. a–d) Comparison between MfGO and HGO, where MfGO was prepared with a residence time of 1.2 min (MfGO-1.2) and 4 min (MfGO-4.0), respectively, in the chip microreactor: a) XPS C1s spectra, b) XRD patterns, c) Raman spectra, d) ^{13}C MAS solid-state NMR spectra, e) FTIR spectra, f) TGA curves with DTG plots.

59 ppm, are assigned as sp^2-hybridized carbon, hydroxyl and epoxide, respectively. The relatively higher peak at 59 ppm indicates relatively more epoxy in MfGO samples. FTIR spectra in Figure 3e show obvious absorption peaks of O—H stretching vibration (≈3433 cm^{-1}), C=O stretching vibration (≈1797 cm^{-1}), C=C vibration from carbon sp^2 bonding or absorbed H_2O molecules (≈1631 cm^{-1}), C—O—C vibration (≈1232 cm^{-1}) and C—O vibrations (≈1405 and ≈1093 cm^{-1}). More epoxide and less carboxyl absorption are observed for MfGOs, consistent with NMR and XPS results. Thermogravimetric analysis (TGA) profiles in Figure 3f show that MfGO samples have the higher thermal weight loss (≈57 wt%) than HGO (≈52 wt%) at 800 °C. The major thermal decomposition of MfGO occurs at lower temperatures, showing the lower thermal stability compared with HGO, as epoxy is less thermally stable and easier to decompose than hydroxyl.[41] All the evidence shows that the oxidization degree in microchannels is higher, leading to more epoxy yet less hydroxyl in MfGO.

The results above have already shown that MfGO can be finely tailored by tuning the resident time in microchannels. With the longer stay of graphite in the microreactor, MfGO-4.0 shows richer wrinkles (Figure S7b, Supporting Information), and larger layer thickness of ≈1.1 nm, yet with slightly smaller lateral size compared to MfGO-1.2 (Figure S7c, Supporting Information). The lower C/O atomic ratio (≈1.8) and increased proportion of hydroxyl and carbonyl groups shows the higher oxidization degree. A comparison of features between MfGO-1.2, MfGO-4.0 and various reported GO samples is listed in Table S3 in the Supporting Information. The microfluidic strategy is also appropriate for the oxidization of flake graphite, as demonstrated in Figure S8 in the Supporting Information. Possibly because of the relatively small diameter of flake graphite, the oxidation reaction was completed within ≈3 min with a yield up to ≈91% (defined as above, evaluated under a centrifugation speed of 3000 rpm). The C/O atomic ratio of graphite oxide from flake graphite is ≈2.9, indicating the lower oxidation degree than the situation when EG is used as the raw material.

PFA capillary has been employed to explore the influence of flow rate by changing the capillary length from 0.5 to 3 m while keeping the resident time near 2 min. As shown in Figure S9a in the Supporting Information, varying the flow rates results in dramatically different exfoliation degree of GO, among which MfGO obtained from 867 µL min^{-1} (denoted as MfGO-P2 in Table S4 in the Supporting Information) shows the higher exfoliation efficiency than those from 226 µL min^{-1} (MfGO-P1) or 1067 µL min^{-1} (MfGO-P3). In contrast to the chip microreactor, MfGOs fabricated in the straight PFA microchannels demonstrate a C/O ratio in a range of 2.6–2.8 (Figure S9b, Supporting Information), using the same EG as the raw material. TGA (Figure S9c, Supporting Information), XRD (Figure S9d, Supporting Information), I_D/I_G (Figure S9e, Supporting Information), UV–vis spectra (Figure S9f, Supporting Information), NMR (Figure S9g, Supporting Information) and FTIR (Figure S9h,

Supporting Information) all show the oxidation degree of MfGOs from straight PFA microchannels slightly increases with the flow rate in the range of study while keeping the similar oxygen-containing functional groups and morphology (SEM and AFM in Figure S10 in the Supporting Information), demonstrating the potential of finely tuning the chemical features of GO in microchannels.

From the fluidic analyses and the characterizations of samples, we can clearly see that the fluidic feature has a profound effect on the graphite oxidation. Among the three steps needed for oxidization of graphite: 1) diffusion of oxidant in bulk solvent to graphite surface, 2) interlayer diffusion of oxidant into the graphite galleries preoccupied by H_2SO_4, and 3) reaction between oxidant and graphite, the sluggish interlayer diffusion of oxidant in step 2) has been considered as the rate-determining step.[19] The rotation of graphite flakes, caused by the enhanced shear rate in the chip microreactor, would improve the mass transfer of oxidant species to graphite surface. At the same time, the increased local shear shall facilitate the exfoliation of graphite oxide, which may further improve the interlayer mass transfer. Since the characteristic time of diffusion (t) can be evaluated by $t = d^2/D$,[31] where d is the diffusion path length and D is the molecule diffusivity, the overall diffusion can be accelerated by the much smaller reactor size and improved mass transfer in the microchannels. Consequently, the oxidization efficiency of graphite has been largely enhanced in chip microchannels. Please note that the rotation of graphite flakes may explain more epoxy groups in MfGO due to more surface reaction (compared to edge reaction), but the shear would readily break the platelets, leading to the smaller platelet size.

As a nondestructive technology, Raman spectroscopy is highly valuable for the structural characterization of carbon materials. The oxidization of graphite in transparent microchannels allows for the use of Raman to in situ monitor the oxidation process. As shown in **Figure 4**a, the laser spot through a commercial Raman spectrometer is focused on a glass microcontainer made by two glass slides sandwiched with a small amount of reaction fluid, or a PFA capillary microreactor, and potentially can be used to detect the chip microreactor, e.g., with help of optical fibers. By observing the appearance of D peak and fitting the G peak (stage-1 H_2SO_4-GIC: 1633–1640 cm^{-1},[19] GO: ≈1590 cm^{-1},[43] and low-functionalization-degree graphene (lfd-G): ≈1572 cm^{-1},[44] inset of Figure 4b) for the graphite in the glass micro-container, the oxidization process can be determined based on the statistical data such as the peak position and full width at the half maximum (FWHM), as shown in Figure 4b. Please notice that, lfd-G, corresponding to the lower functionalization and no more intercalation by sulfuric acid,[44] owns much narrower G/D bands and relatively constant D/G ratio of ≈1, in addition to the G peak position different from

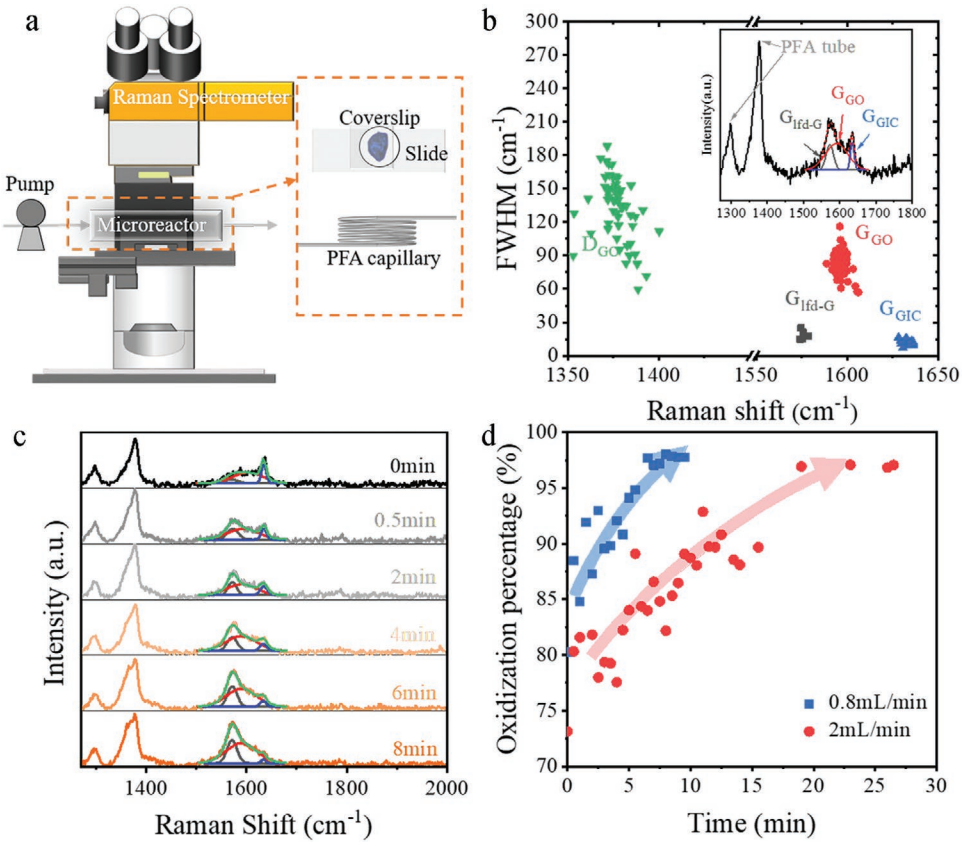

Figure 4. a) Schematic of the experiment setup for in situ Raman measurement on the microreactors (slide and coverslip, PFA capillary). b) Statistics of peak position and FWHM of G and D peaks of oxidized graphite flakes (5 lfd-G, 59 GO, and 47 H_2SO_4-GIC). Inset shows the typical fitting of G peak. c) Raman evolution of graphite with oxidation in a PFA capillary (flow rate: 0.8 mL min^{-1}) at the room temperature. d) Oxidization degree depending on the volume rate in a PFA capillary at the room temperature.

GO. To observe the changes in Raman spectrum more clearly, a PFA capillary (length: 0.8 m) was used to circularly perform the reaction at the room temperature with different flow rates, as depicted in Figure S11a,b in the Supporting Information. Figure 4c shows the Raman evolution for the flow rate of ≈800 µL min^{-1}. We can see that, with the proceeding of oxidization, the G-band of stage-1 H_2SO_4-GIC gradually weakens till it nearly disappears after 6 mins, accomplished by a significant enhancement of G-bands from GO and lfd-G. Similar transition was also observed in the case when the flow rate was set at 2 mL min^{-1} as shown in Figure S11c in the Supporting Information, where it took ≈18 min to reach the complete oxidization. By calculating the area fraction of G-bands of GO and lfd-G, the oxidization degree could be estimated with time for different flow rates, as shown in Figure 4d. By assuming that graphite flake is an ideal tabular cylinder, a kinetic equation, $-1-(1-\alpha)^{1/2}=kt$, is used to judge the reaction,[45] in which α is conversion rate (oxidization percentage) and k is the reaction rate constant. From the data in Figure 4d, a reaction rate constant k of 0.029 is estimated for the flow rate of 800 μL min^{-1}, while 0.011 for the flow of 2 mL min^{-1}, consistent with the results shown in Figure S9 in the Supporting Information, i.e., the flow rate would have a prominent influence on the reaction in PFA capillary tubes. In addition, the influence of raw graphite has been investigated with in situ Raman spectroscopy, based on EG and flake graphite with different sizes for each (SEM images in Figure S12 in the Supporting Information), as shown in spectra in Figure S13 in the Supporting Information. As summarized in Figure S14 and Table S6 in the Supporting Information, we can see the clear dependence of the oxidization kinetics on the size and the oxygen content in the raw graphite. Analysis based on the Raman data provides potentially useful index which can be used to trace the oxidization in continuous production of graphite oxide in microchannels.

Sticking to the microfluidic strategy, next we demonstrate that MfGO can be assembled or reduced in microchannels. As shown in **Figure 5**a, MfGO gel fibers can be obtained through a shear-induced regular alignment of MfGO platelets in a PFA microchannel (inner diameter: 1 mm), followed by immersed in a coagulation bath (5 wt% $CaCl_2$) for divalent ionic cross-linking.[46] After the residual coagulation solution was washed in a water bath, the collected gel fibers were dried at 60 °C overnight and wound on a poly(tetrafluorothylene) (PTFE) drum. The dried 100 µm-thick MfGO fiber exhibits a compact yet wrinkled surface under SEM. Figure 5b shows the microfluidic reduction of MfGO assisted by L-ascorbic acid (L-AA), by pumping the mixture of MfGO (1 mg mL^{-1}) and L-AA into a 3 m long PFA microchannel (inner diameter: 1 mm) maintained at 90 °C in an oil bath. The color in the PFA tube gradually darkens along the flow direction; the gloomy suspension is finally collected, purified and dried, named as MfrGO, showing a crumpled morphology, as viewed in Figure S15a in the Supporting Information. The XPS spectra in Figure S15b in the Supporting Information demonstrate that the oxygen-containing functional groups have been effectively removed. Compared with MfGO (I_D/I_G = 0.91), the I_D/I_G ratio of MfrGO powder is increased to 1.23 (Figure S15c, Supporting Information), indicating the higher quantity of structural defects after reduction.[47] The successful assembly and reduction of MfGO in microchannels allow for the integrity of preparation and post treatment of GO all the way in a continuous manner.

Finally, highly oriented films have been prepared by vacuum filtrating MfGO and the following reduction, carbonization, and graphitization at high temperatures (details in Experiential Section).[39] The well-aligned structure of the film is confirmed by the cross-section SEM image as shown in the inset of Figure 5c; the shiny surface, vanishing Raman D peak and sharp XRD diffusion peak (Figure S16, Supporting Information) demonstrate the high-crystalline feature of the film obtained. As shown in Figure 5c, in the preliminary testing the film with a thickness of ≈10 µm demonstrates thermal and electrical conductivities of 1155 W m^{-1} K^{-1} and 1.1 × 10^6 S m^{-1}, comparable to recently reported results,[48,49] which indicates the promising applicability of MfGO for heat dissipation or electrical conductance.[50]

3. Conclusion

We have developed a fast and safe continuous flow synthesis of GO through microfluidic strategy. The preparation has been achieved in minutes, much faster than the modified Hummers' method yet with a comparable exfoliation yield and chemical features, leading to graphene films with practically useful thermal and electrical conductivities. We have proved that the

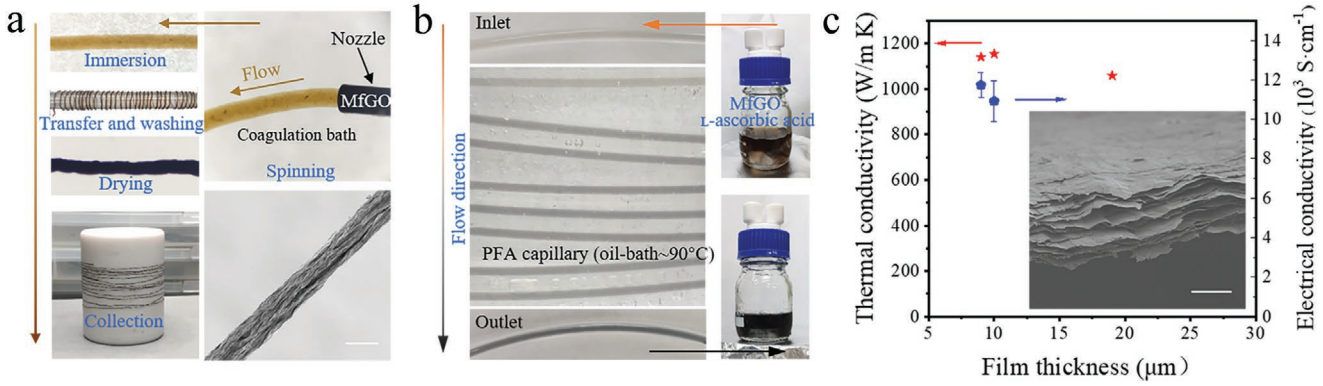

Figure 5. a) Microfluidic assembly and SEM image of MfGO fibers by the PFA capillary. b) Microfluidic reduction of MfGO with L-AA in the PFA capillary. c) Thermal and electrical conductivity and SEM image (inset) of a film made from MfGO. Scale bars: a) 100 µm, c) 20 µm.

continuous flow in microchannels has significantly improved the oxidation efficiency due to the enhanced diffusion of reactant and highly efficient energy transfer, especially in purposely designed chip reactors. The transparent microchannels have provided the better opportunity for one to on-line monitor the preparation by Raman microscopy. The assembly and reduction in microchannels would further expand the ability of integrating the microfluidic strategy for various graphene products. We believe that the microfluidic strategy in the current work would revolute the traditional batch-style preparation of graphene materials, towards future production lines with high integrity and intelligence, based on the dynamic data collection and analysis during the fluidic reactions.

4. Experimental Section

Materials: Expandable graphite (EG, mean particle size: ≈75 µm) and flake graphite (G, >100 mesh) were purchased from Aladdin. Another flake graphite (mean particle size: ≈42 µm) was purchased from Qingdao Tianheda Graphite Co., Ltd. (Qingdao, China). Potassium permanganate ($KMnO_4$), sulfuric acid (H_2SO_4, 96–98 wt%), hydrogen peroxide (H_2O_2), L-ascorbic acid (L-AA) and calcium chloride ($CaCl_2$) were purchased from Sinopharm Chemical Reagent Co., Ltd., and used without further purification.

Microfluidic Oxidation of Graphite: In a typical microfluidic synthesis, 1 g EG was dispersed in concentrated H_2SO_4 (50 mL) in a sealed screw-top bottle, and the suspension was stirred vigorously for 30 min. Keeping the dispersion below 5 °C by an ice-bath, $KMnO_4$ was added in small portions to the bottle in over 10 min and the suspension was stirred for additional 1 h. The mixing suspension was then pumped into the microreactor by a peristaltic pump with different volumetric flow rates. A custom-designed chip (channel size: 0.7–1.0 mm, volume: ≈1.2 mL) or polyfluoroalkoxy (PFA) capillary (inner diameter: 1 mm) were used as microchannels. During the oxidization, the whole microreactor was kept at 35 °C by water-bath. The resident time was regulated by changing volumetric flow rate. For instance, the reaction time of 1.2 min corresponds to a flow rate of 1 mL min^{-1}. The reaction mixture (40 mL) was collected and kept in an ice bath, then deionized (DI) water (80 mL, twice the volume of the collected mixture) was slowly added into the obtained mixture, followed by the addition of H_2O_2 (≈4 mL) till gas evolution completed. The obtained graphite oxide was separated immediately and washed by HCl solution (10 vol.%) twice by centrifugation. Subsequently the collected graphite oxide was further purified by repeated centrifugation (11 000 rpm) and re-dispersion till the supernatant was neutral. Finally, MfGO was obtained after mild sonication using a bath sonication (5 min, 125 W). The suspension was then centrifuged for 1 h at 3000 rpm (1006 g) to remove the unexfoliated graphite oxide particles. The yield was calculated by calculating the mass ratio of GO freeze-dried from the centrifugation supernatant to the total mass.

Flask Oxidation of Graphite: The modified Hummers' method was carried out in a flask. Fully dried EG powder (3 g) was added in concentrated H_2SO_4 (70 mL) and stirred for 30 min, then $KMnO_4$ (9 g) was added into the mixture slowly under ice bath. The reaction suspension was heated to 35 °C and maintained for 2 h. After that, the further oxidation was initiated by adding DI water (150 mL) dropwise and kept at 95 °C for 15 min. The reaction was terminated by pouring 300 mL water and addition of 15 mL H_2O_2. The same purification process was carried out to obtain HGO.

Real-Time Observation of the Motion of Graphite Flakes: To clearly observe individual graphite particles in chip microchannels, EG powder (0.1 g) was dispersed in 50 mL concentrated H_2SO_4, then $KMnO_4$ (0.3 g) was added under ice-bath. The flow rate was set at relatively low value of 0.1 mL min^{-1}. For better observation, the playback speed in the supporting videos was slowed down to 1/10 of the normal speed.

Numerical Simulation of Fluid Dynamics in Microchannels: The dynamic of the velocity field **v** is described by the Navier–Stokes equation of the incompressible non-Newtonian fluid with a unity matrix **I**

$$\nabla \cdot \nu = 0 \tag{1}$$

$$\rho(\nu \cdot \nabla)\nu = \nabla \cdot [-pI + \mu(\nabla\nu + \nabla\nu^T] \tag{2}$$

Firstly, two microchannel geometric parameters were built in the software and the situation of pure H_2SO_4 was studied. The density and dynamic viscosity of pure H_2SO_4 used are 1826.5 kg m^{-3} and 0.0171 Pa s, respectively, corresponding to the situation of 30 °C. The area of finite element was generated based on the specific microchannel geometry. From the simulation, shear rate and velocity distribution were obtained.

Microfluidic Assembly of MfGO Fibers: The highly concentrated MfGO dispersion was prepared by centrifugal concentration at 11 000 rpm for 10 min. Then, the spinning dope passed through the nozzle (with an inner diameter of 300 µm) at a flow rate of 90 µL min^{-1} into the $CaCl_2$ coagulation bath (5 wt%). After the gel fibers were transferred to a water bath to remove residual ions and dried in an oven at 60 °C overnight, the resulting graphene fibers were collected on a poly(tetrafluoroethylene) (PTFE) drum with a diameter of 4 cm.

Microfluidic Reduction of MfGO: Typically, the freeze-dried MfGO powder was re-dispersed to 1 mg mL^{-1} suspension, followed by ultrasonic treatment for 30 min with a power of 200 W and sieving through a 600-mesh sieve to separate the precipitate. After adding L-ascorbic acid powder into the MfGO suspension (0.88 g L-ascorbic acid per 1 g MfGO) and stirring for 10 min, the mixture was pumped into the PFA capillary microchannel with a length of 3 m, and the temperature was maintained at 90 °C by hot water bath. In a typical procedure, the flow rate was set at 212 µL min^{-1}, and the corresponding resident time was 11.1 min. The reaction suspension was collected from outlet, and the powder sample was obtained through filtration and subsequent purification by washing with water and acetone three times each.

Fabrication and Measurements of Graphene Films: For the preparation of thermally or electrically conductive films, thick MfGO films were obtained by stacking several wet thin MfGO films (typically 20–30 µm in thickness) made by vacuum filtration. The reduction, carbonization and graphitization procedure has been described in our previous reports.[39] Firstly, MfGO films were annealed to 300 °C with a heating rate of 2 °C min^{-1} and kept for 2 h to partially remove the oxygen-containing functional groups, and then heated to 1000 °C with heating rate of 5 °C min^{-1} and maintained for 1 h. Subsequently, the pre-treated films were sequentially annealed at 2000 and 2800 °C each for 2h. Finally, the obtained graphene films were mechanically pressed under ≈75 MPa using a dynamic flat presser for further densifying.

Thermal conductivity (K) was obtained by multiplying the specific heat capacity (C_p, J g^{-1} K^{-1}), film density (ρ, g cm^{-3}) and thermal diffusivity coefficient (α, mm^2 s^{-1}), namely $K = \rho C_p \alpha$.

Characterizations: The morphology of GO platelets was characterized by field-emission SEM (Hitachi SU8220, Japan), HRTEM (JEOL-2100F, Japan) and AFM (Nanoscope III MultiMode, Germany). The structural characteristics of GO platelets were evaluated by Raman spectroscopy (LabRAM, RM3000, Renishaw, UK) with a 532 nm laser, XRD with Cu K_α radiation (λ = 1.5406 Å, tube voltage = 40 kV, tube current = 30 mA, Rigaku SmartLab, Japan) and UV/Vis absorption spectra (UV-2600, SHIMADZY, Japan). The chemical composition of GO was analyzed by XPS (Thermo ESCALAB 250, USA) with Al K_α radiation ($h\nu$ = 1486.6 eV) and TGA under N_2 atmosphere with a heating rate of 10 °C min^{-1} (TG 209F1 Iris, Netzsch, Germany). The oxygen-containing functional groups were evaluated by FTIR (attenuated total reflection mode, Thermo Nicolet nexus-470, US) and SSNMR spectra (Bruker Avance 600WB, 100.7 MHz for ^{13}C nuclei, bore size of 4 mm, MAS rate of 7 kHz). The electrical conductivity of graphene films was measured by a four-probe testing system (Keithley 2182A/6430, USA). The thermal conductivity was evaluated by Hyper laser flash (NETZSCH LFA 467, Germany).

Real-Time Raman Spectroscopy: The real-time structure evolution of graphite in microchannels was monitored by in situ Raman spectroscopy (LabRAM, RM3000, Renishaw, UK) with a 532 nm laser. The microscope was focused on the center of the microchannel at low magnification. The integral time was set as 1s while the laser power was set at 50 mW. During the real-time monitoring in different flow rate, the microchannel was maintained at room temperature of ≈22 °C. The flow rate was kept at 800 μL min^{-1} for comparison of four kinds of raw graphite, and its temperature was maintained at ≈15 °C. In view of the high flow velocity of up to several centimeters per second in the microchannel, the thermal effect caused by the laser may be ignored.

Statistical Analysis: Without pre-processing of data, based on the Raman spectra of 5 lfd-G, 59 GO, and 47 H_2SO_4-GIC, the average G peak position (1574.7 ± 1.3 cm^{-1} for lfd-G, 1596.6 ± 3.1 cm^{-1} for GO, and 1634.2 ± 1.8 cm^{-1} for H_2SO_4-GIC) and FWHM (18.7 ± 3.5 cm^{-1} for lfd-G, 81.6 ± 10.5 cm^{-1} for GO, 11.4 ± 1.8 cm^{-1} for H_2SO_4-GIC) were obtained. The fitting of the G peak was performed using the peak analyzer program in Origin 2019.

Supporting Information

Supporting Information is available from the Wiley Online Library or from the author.

Acknowledgements

This work was supported by National Key R&D Program of China (Grant Nos. 2020YFA0711502) and Natural Science Foundation of China (Nos. 51772282, 51972299, 52003265). B.Q. and Y.Z. thank the support of Key R&D Program of Jiangsu Province of China (BE2021007-1).

Conflict of Interest

The authors declare no conflict of interest.

Author Contributions

C.Y. and G.W. contributed equally to this work. Y.Z. and C.Y. conceived the experiments. C.Y. conducted the preparation experiments, data analysis and drafted the manuscript. G.W. and Z.T. designed the chip microreactor and helped to conduct the reaction fluid analysis. H.Y. helped to analyze the characterization of GO. J.L. helped to analyze the mass transfer in microchannel. K.N. helped to analyze experimental data. F.P. helped to analyze the NMR data. M.G. helped to analyze the reduction of GO. Y.W. conducted the measurement of thermal conductivity of graphene films. H.J., F.Z., B.Q., and Y.Z. supervised the study and revised this manuscript. All authors discussed the results and commented on the manuscript.

Data Availability Statement

The data that support the findings of this study are available from the corresponding author upon reasonable request.

Keywords

continuous preparation, graphite oxide, microchannels, microreactors, on-line monitoring

Received: September 7, 2021
Revised: January 28, 2022
Published online: March 2, 2022

[1] S. Zheng, Q. Tu, M. Wang, J. J. Urban, B. Mi, *ACS Nano* **2020**, *14*, 6013.
[2] H. Sun, Z. Xu, C. Gao, *Adv. Mater.* **2013**, *25*, 2554.
[3] D. A. Dikin, S. Stankovich, E. J. Zimney, R. D. Piner, G. H. B. Dommett, G. Evmenenko, S. T. Nguyen, R. S. Ruoff, *Nature* **2007**, *448*, 457.
[4] Z. Xu, Y. Zhang, P. Li, C. Gao, *ACS Nano* **2012**, *6*, 7103.
[5] Y. Zhu, S. Murali, M. D. Stoller, K. J. Ganesh, W. Cai, P. J. Ferreira, A. Pirkle, R. M. Wallace, K. A. Cychosz, M. Thommes, D. Su, E. A. Stach, R. S. Ruoff, *Science* **2011**, *332*, 1537.
[6] X. Yang, C. Cheng, Y. Wang, L. Qiu, D. Li, *Science* **2013**, *341*, 534.
[7] J. Abraham, K. S. Vasu, C. D. Williams, K. Gopinadhan, Y. Su, C. T. Cherian, J. Dix, E. Prestat, S. J. Haigh, I. V. Grigorieva, P. Carbone, A. K. Geim, R. R. Nair, *Nat. Nanotechnol.* **2017**, *12*, 546.
[8] K. P. Loh, Q. Bao, G. Eda, M. Chhowalla, *Nat. Chem.* **2010**, *2*, 1015.
[9] T. Ramanathan, A. A. Abdala, S. Stankovich, D. A. Dikin, M. Herrera-Alonso, R. D. Piner, D. H. Adamson, H. C. Schniepp, X. Chen, R. S. Ruoff, S. T. Nguyen, I. A. Aksay, R. K. Prud'Homme, L. C. Brinson, *Nat. Nanotechnol.* **2008**, *3*, 327.
[10] S. Liu, T. H. Zeng, M. Hofmann, E. Burcombe, J. Wei, R. Jiang, J. Kong, Y. Chen, *ACS Nano* **2011**, *5*, 6971.
[11] Y. Zhu, S. Murali, W. Cai, X. Li, J. W. Suk, J. R. Potts, R. S. Ruoff, *Adv. Mater.* **2010**, *22*, 3906.
[12] B. C. Brodie, *Proc. Royal Soc. London* **1859**, *10*, 11.
[13] L. Staudenmaier, *Ber. Dtsch. Chem.* **1898**, 1481.
[14] W. S. Hummers, R. E. Offeman, *J. Am. Chem. Soc.* **1958**, *80*, 1339.
[15] Y. Zhu, Y. Ma, R. Tang, *Preparation and Application of Graphene Oxide*, Chemical Industry Press, Beijing, **2019**.
[16] D. C. Marcano, D. V. Kosynkin, J. M. Berlin, A. Sinitskii, Z. Sun, A. Slesarev, L. B. Alemany, W. Lu, J. M. Tour, *ACS Nano* **2010**, *4*, 4806.
[17] K. R. Koch, *J. Chem. Educ.* **1982**, *59*, 973.
[18] S. Lee, S. H. Eom, J. S. Chung, S. H. Hur, *Chem. Eng. J.* **2013**, *233*, 297.
[19] A. M. Dimiev, J. M. Tour, *ACS Nano* **2014**, *8*, 3060.
[20] S. Seiler, C. E. Halbig, F. Grote, P. Rietsch, F. Börrnert, U. Kaiser, B. Meyer, S. Eigler, *Nat. Commun.* **2018**, *9*, 836.
[21] L. Peng, Z. Xu, Z. Liu, Y. Wei, H. Sun, Z. Li, X. Zhao, C. Gao, *Nat. Commun.* **2015**, *6*, 5716.
[22] J. Cao, P. He, M. A. Mohammed, X. Zhao, R. J. Young, B. Derby, I. A. Kinloch, R. A. W. Dryfe, *J. Am. Chem. Soc.* **2017**, *139*, 17446.
[23] S. Pei, Q. Wei, K. Huang, H. Cheng, W. Ren, *Nat. Commun.* **2018**, *9*, 145.
[24] Y. Zhu, H. Ji, H. Cheng, R. S. Ruoff, *Natl. Sci. Rev.* **2018**, *5*, 90.
[25] M. AlAmer, A. R. Lim, Y. L. Joo, *Ind. Eng. Chem. Res.* **2018**, *58*, 1167.
[26] G. Laudadio, Y. Deng, K. van der Wal, D. Ravelli, M. Nuño, M. Fagnoni, D. Guthrie, Y. Sun, T. Noël, *Science* **2020**, *369*, 92.
[27] C. W. Coley, M. Abolhasani, H. Lin, K. F. Jensen, *Angew. Chem., Int. Ed.* **2017**, *56*, 9847.
[28] K. F. Jensen, B. J. Reizman, S. G. Newman, *Lab Chip* **2014**, *14*, 3206.
[29] D. Dallinger, B. Gutmann, C. O. Kappe, *Acc. Chem. Res.* **2020**, *53*, 1330.
[30] B. J. Reizman, K. F. Jensen, *Acc. Chem. Res.* **2016**, *49*, 1786.
[31] Y. Mo, Z. Lu, G. Rughoobur, P. Patil, N. Gershenfeld, A. I. Akinwande, S. L. Buchwald, K. F. Jensen, *Science* **2020**, *368*, 1352.
[32] P. G. Karagiannidis, S. A. Hodge, L. Lombardi, F. Tomarchio, N. Decorde, S. Milana, I. Goykhman, Y. Su, S. V. Mesite, D. N. Johnstone, R. K. Leary, P. A. Midgley, N. M. Pugno, F. Torrisi, A. C. Ferrari, *ACS Nano* **2017**, *11*, 2742.
[33] H. Qiu, X. Wu, R. Hong, G. Wu, S. Chen, *Energy Fuels* **2020**, *34*, 11519.
[34] G. Wu, P. Tan, X. Wu, L. Peng, H. Cheng, C. F. Wang, W. Chen, Z. Yu, S. Chen, *Adv. Funct. Mater.* **2017**, *27*, 1702493.
[35] R. L. Hartman, J. P. McMullen, K. F. Jensen, *Angew. Chem., Int. Ed.* **2011**, *50*, 7502.

[36] G. Wang, Y. Gu, L. Zhao, J. Xuan, G. Zeng, Z. Tang, Y. Sun, *Chem. Eng. Sci.* **2019**, *195*, 250.
[37] S. Panić, S. Loebbecke, T. Tuercke, J. Antes, D. Bošković, *Chem. Eng. J.* **2004**, *101*, 409.
[38] R. Rusconi, H. A. Stone, *Phys. Rev. Lett.* **2008**, *101*, 254502.
[39] H. Yuan, J. Ye, C. Ye, S. Yin, J. Li, K. Su, G. Fang, Y. Wu, Y. Zheng, M. Ge, R. Tang, G. Feng, Y. Qu, Y. Zhu, *Chem. Mater.* **2021**, *33*, 1731.
[40] H. Chen, W. Du, J. Liu, L. Qu, C. Li, *Chem. Sci.* **2019**, *10*, 1244.
[41] J. H. Kang, T. Kim, J. Choi, J. Park, Y. S. Kim, M. S. Chang, H. Jung, K. T. Park, S. J. Yang, C. R. Park, *Chem. Mater.* **2016**, *28*, 756.
[42] A. C. Ferrari, D. M. Basko, *Nat. Nanotechnol.* **2013**, *8*, 235.
[43] K. N. Kudin, B. Ozbas, H. C. Schniepp, R. K. Prud'Homme, I. A. Aksay, R. Car, *Nano Lett.* **2008**, *8*, 36.
[44] A. M. Dimiev, K. Shukhina, A. Khannanov, *Carbon* **2020**, *166*, 1.
[45] C. Li, Y. Shi, X. Chen, D. He, L. Shen, N. Bao, *Chem. Eng. Sci.* **2018**, *176*, 319.
[46] Z. Xu, H. Sun, X. Zhao, C. Gao, *Adv. Mater.* **2013**, *25*, 188.
[47] C. Gómez-Navarro, J. C. Meyer, R. S. Sundaram, A. Chuvilin, S. Kurasch, M. Burghard, K. Kern, U. Kaiser, *Nano Lett.* **2010**, *10*, 1144.
[48] H. Huang, X. Ming, Y. Wang, F. Guo, Y. Liu, Z. Xu, L. Peng, C. Gao, *Carbon* **2021**, *180*, 197.
[49] S. Chen, Q. Wang, M. Zhang, R. Huang, Y. Huang, J. Tang, J. Liu, *Carbon* **2020**, *167*, 270.
[50] Y. Zhu, B. Qu, D. V. Andreeva, C. Ye, K. S. Novoselov, *Mater. Today* **2021**, *47*, 9.